Designing High-Permittivity Pads for Dielectric Shimming in MRI using Model Order Reduction and Gauss-Newton Optimization

J.H.F. van Gemert* W.M. Brink† A.G. Webb† R.F. Remis*

Abstract — **High-field MRI reduces the homogeneity of the B_1^+ transmit field, which in turn degrades the quality of MR images. High-permittivity pads are increasingly used to restore the homogeneity of this transmit field. Designing such a pad in terms of dimensions, position, and constitution is not trivial, however, and in this work we propose a design method that can be used to find an optimal pad for a certain imaging region of interest. By incorporating a projection based model order reduction technique in a Gauss-Newton optimization method, optimal dielectric pads can be found at significantly reduced computation times. We illustrate the performance of our optimization method by designing a pad for 7T cerebellum imaging and show its effectiveness in an actual MR imaging experiment.**

1 INTRODUCTION

Stronger static background fields in magnetic resonance imaging (MRI) lead to an increased Signal to Noise (SNR) ratio and consequently to reduced scanning times or an increase in the spatial resolution of an MR scan [1]. The RF frequency required to obtain an MR signal increases linearly with the magnitude of this static background field. A field strength of 3T, for example, requires an RF frequency of 128 MHz, whereas for 7T this frequency is equal to 298 MHz.

A high-quality MR scan can be acquired if the transmitted RF field is homogeneous and if its magnitude is sufficiently large. More specifically, it is the forward circularly polarized magnetic flux component that should meet these criteria. This component is defined as $B_1^+ = \frac{B_x + \mathrm{j}B_y}{2}$, where j is the imaginary unit, and B_x and B_y are the transverse x- and y-components of the magnetic flux density phasor.

For higher field strengths, the wavelength of the RF field decreases and consequently causes wavelength effects that reduce the uniformity of the B_1^+ field. In turn, weak magnetic field regions translate into reduced contrast thereby degrading the quality of an MR scan as illustrated in Fig. 1a.

Many methods have been published that try to overcome the non-uniformity in the region of interest (ROI) [2, 3], but most of them have not been used in the clinic for safety reasons due to the uncertainty of power deposition in the patient. Alternatively, safe, low-cost, and easy-to-use dielectric pads can also be used to minimize the nonuniformity of the B_1^+ field. Typical pads have a high relative permittivity up to 300 and are placed in the vicinity of the ROI. When properly designed, the uniformity can be significantly improved as shown in [4]-[6], for example.

Designing dielectric pads is not straightforward, however, as it depends on the transmit antennas, the ROI, and the patient. Conventionally, the MR configuration is build in an electromagnetic field solver and the RF response for a wide variety of dielectric pads is evaluated. Since the computational domain and the pad parameter space (dimensions, position, and constitution) are very large, the associated computation times are very long as well.

Previously, we proposed a method to significantly speed up the B_1^+ evaluation of dielectric pads [7]. The method exploits the property that for each simulation, the RF coil, RF shield, and the heterogeneous body model remains fixed (as illustrated in Fig. 2a for cerebellum imaging). The only part that changes throughout the simulations is the relatively small dielectric pad. To exploit this feature, a pad "design domain" is defined to which every pad should be confined as illustrated in Fig. 2b. Employing a scattering formalism, it is then possible to compute the perturbation due to any pad efficiently. Although this method is fast, it does not offer an actual design method.

In this paper, we extend the above mentioned B_1^+ field evaluation method to a full three-dimensional pad optimization technique. Specifically, first we describe a high-permittivity pad in terms of a small set of pad design parameters and subsequently construct projection based reduced order models for the B_1^+ fields. These models have an order that is much smaller than the order of the original unre-

*Circuits and Systems Group, Faculty of Electrical Engineering, Mathematics and Computer Science, Delft University of Technology, e-mail: J.H.F.vanGemert-1@tudelft.nl, R.F.Remis@tudelft.nl.

†C.J. Gorter Center for High Field MRI of the Leiden University Medical Center, email: A.Webb@lumc.nl, W.M.Brink@lumc.nl.

978-1-5090-4451-1/17/$31.00 ©2017 IEEE

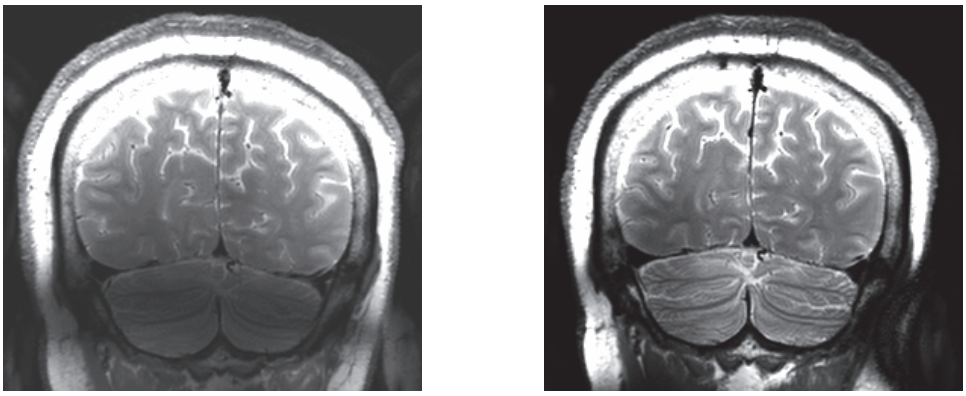

(a) (b)

Figure 1: T2-weighted turbo spin echo head scans of the brain at 7T (298 MHz). Signal voids are encountered in the cerebellum and temporal lobes due to non-uniformity in the B_1^+ transmit field. Scans have been obtained on a 7T Philips Achieva, where a quadrature head coil is used for transmission and a 32 channel receive array for reception.

duced system and can be evaluated very efficiently for a given set of pad design parameters. Subsequently, the reduced order models are incorporated in a Gauss-Newton optimization approach to efficiently determine an optimal pad that minimizes the 2-norm of a nonlinear residual defined over the domain of interest. Finally, as an illustrative example, we apply our optimization technique to design a pad for cerebellum imaging at 7T [10].

2 METHODS

Our pad design approach is based on a scattering formalism, in which the total discretized B_1^+ field is written as a superpostion of the B_1^+ field in a configuration without a dielectric pad and a scattered field that is due to the presence of the pad. Explicitly, the spatially discretized B_1^+ field is written as [7]

$$\mathsf{b}_1^+(\mathsf{c}) = \mathsf{b}_1^{+;\text{no pad}} + \mathsf{G}^{B_1^+\mathrm{J}}\mathsf{j}(\mathsf{c}), \tag{1}$$

where the first term on the right-hand side is the background B_1^+ field in absence of a dielectric pad, while the second term represents the scattered field with $\mathbf{j}$ the electric current density state vector defined as

$$\mathsf{j}(\mathsf{c}) = \left[\mathsf{I}_P - \mathsf{X}_{\text{pad}}(\mathsf{c})\mathsf{G}^{\mathrm{EJ}}\right]^{-1}\mathsf{X}_{\text{pad}}(\mathsf{c})\mathsf{e}^{\text{no pad}}, \tag{2}$$

and $\mathsf{e}^{\text{no pad}}$ the background electric field strength. A pad is completely characterized by prescribing the dielectric pad parameters at every electric grid edge inside the pad design domain and by putting the contrast parameters

$$c_p = \sigma(\mathbf{r}_{k_p}) + \mathrm{j}\omega\varepsilon_0[\varepsilon_{\mathrm{r}}(\mathbf{r}_{k_p}) - 1], \tag{3}$$

on the diagonal of the diagonal contrast matrix X_{pad} for $p = \{1, 2, \ldots, P\}$, where P is the number of grid edges in the pad design domain. Finally, $\mathsf{G}^{B_1^+\mathrm{J}}$ and G^{EJ} are the discretized Green's tensors of the inhomogeneous background mapping the electric current to B_1^+ and electric fields, respectively. This formalism is efficient since the system that needs to be solved for every dielectric pad is of order P, which is much smaller than the total number of grid edges N present inside the total computational domain.

2.1 Subdomains and parametrization

In its current form, Eq. (1) allows for dielectric grid edge variations within a pad and pads of any shape can be modeled using this equation. In practice, however, such fine-scale variations are not required and only rectangular pads with constant material parameters can be fabricated easily. Therefore, the pad design domain is divided in non-overlapping rectangular subdomains as shown in Fig. 2c, where each subdomain accumulates edges belonging to that particular domain. Hereafter, the model from Eq. (1) is parameterized such that solely rectangular pads can be modeled. The pad parameters are given by

$$\mathsf{p} = \left[z_{\mathrm{B}}, z_{\mathrm{T}}, \phi_{\mathrm{L}}, \phi_{\mathrm{R}}, \varepsilon_{\mathrm{r}}\right]^T, \tag{4}$$

where the first four parameters control the dimensions and position of the pad as shown in Fig. 2d, and ε_{r} determines the relative permittivity of the pad. By introducing the subdomains and the parameterization of Eq. (4), the parameterized state

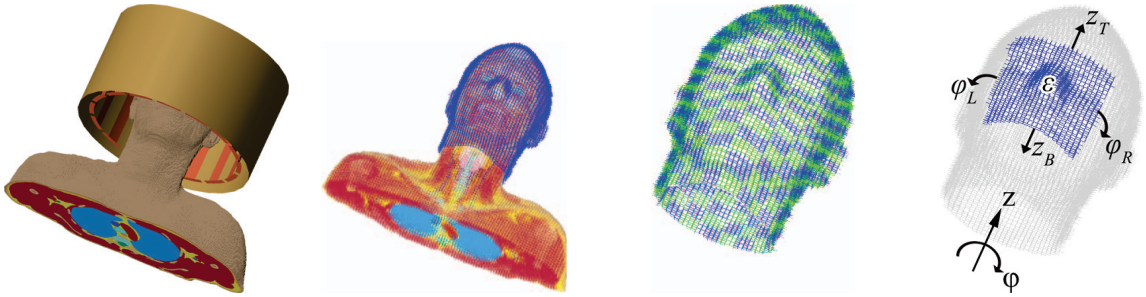

Figure 2: Head and shoulders of the male body model Duke, head coil, and shield used for enhanced imaging of the cerebellum (a). The pad design domain defined all around the head model (b). Pad design domain subdivided into subdomains (c). Illustration of the pad design parameters (d).

vector

$$\mathsf{j}(\mathsf{p}) = \left[\mathsf{I}_P - \sum_{i=1}^{D} \mathsf{f}_i(\mathsf{p})\mathsf{G}_i^{\mathrm{EJ}}\right]^{-1} \sum_{i=1}^{D} \mathsf{f}_i(\mathsf{p})\mathsf{X}_{\mathrm{pad};i}\mathsf{e}^{\text{no pad}}, \quad (5)$$

is obtained, where $\mathsf{G}_i^{\mathrm{EJ}}$ and $\mathsf{X}_{\mathrm{pad};i}$ are the columns of the full Green's tensor G^{EJ} and contrast matrix $\mathsf{X}_{\mathrm{pad}}$ that belong to subdomain i, with $i = \{1, 2, \ldots D\}$ and D the number of subdomains. Furthermore, $\mathsf{f}_i(\mathsf{p})$ is a contrast function that maps the parameters to the material values for each subdomain (for details, see [8]).

2.2 Reduced order model

To evaluate the parameterized current density of Eq. (5), the solution of a system of order P is required for each pad realization. The order of this system can be reduced by removing possible redundant data that may be present in our system. We follow a Projection Based Model Reduction approach to eliminate this possible redundancy [9]. Specifically, we approximate the parameterized current density of Eq. (5) by the reduced order model

$$\mathsf{j}_r(\mathsf{p}) = \mathsf{U}_r\mathsf{a}_r(\mathsf{p}), \quad (6)$$

where U_r is an orthogonal basis matrix and a_r is the vector of expansion coefficients. The basis U_r is obtained by first acquiring a snapshot matrix S defined as

$$\mathsf{S} = [\mathsf{j}_1(\mathsf{p}_1) \ldots \mathsf{j}_S(\mathsf{p}_S)], \quad (7)$$

where every column j_i is the current density of a randomly chosen design vector p_i, for $i = \{1, 2, \ldots, S\}$ and S the number of snapshots. Subsequently, the thin singular value decomposition is computed for matrix S after which the r most significant left singular vectors are extracted to form our new basis U_r. To find the coefficients a_r we require that the residual of the reduced order model is orthogonal to the basis U_r, that is, we impose the Galerkin condition to find

$$\mathsf{a}_r(\mathsf{p}) = \left[\mathsf{I}_r - \sum_{i=1}^{D} \mathsf{f}_i(\mathsf{p})\mathsf{G}_i^{\mathrm{EJ};r}\right]^{-1} \sum_{i=1}^{D} \mathsf{f}_i(\mathsf{p})\mathsf{X}_{\mathrm{pad};i}^{r}\mathsf{e}^{\text{no pad}},$$

where $\mathsf{G}_i^{\mathrm{EJ};r} = \mathsf{U}_r^H\mathsf{G}_i^{\mathrm{EJ}}\mathsf{U}_r$ and $\mathsf{X}_{\mathrm{pad};i}^{r} = \mathsf{U}_r^H\mathsf{X}_{\mathrm{pad};i}$ are the reduced matrices. Combining the obtained results gives us the reduced order model

$$\mathsf{b}_1^{+;r}(\mathsf{p}) = \mathsf{b}_1^{+;\text{no pad}} + \mathsf{G}^{B_1^+\mathrm{J};r}\mathsf{a}_r(\mathsf{p}). \quad (8)$$

Note that to compute the expansion coefficients we only have to solve a system of order r instead of order P.

2.3 Pad design

To find a pad that increases the B_1^+ uniformity within an ROI, we minimize the cost functional

$$C(\mathsf{p}) = \frac{1}{2}\frac{\|\mathsf{b}_1^{+;r}(\mathsf{p}) - \mathsf{b}_1^{+;\text{desired}}\|_{2;\mathrm{ROI}}^2}{\|\mathsf{b}_1^{+;\text{desired}}\|_{2;\mathrm{ROI}}^2}, \quad (9)$$

over all feasible pad parameters vectors p. This implies that the discrepancy between a desired B_1^+ field $\mathsf{b}_1^{+;\text{desired}}$ and modeled field $\mathsf{b}_1^{+;r}(\mathsf{p})$ in a certain ROI is minimized. The optimal dielectric pad is found by using the Gauss-Newton algorithm.

3 IMPLEMENTATION AND RESULTS

To illustrate the performance of our pad design approach, we optimize a dielectric pad for cerebellum imaging at 7T (298 MHz). First, the configuration as shown in Fig 2a is constructed on a 5 mm^3 grid in Remcom XFdtd in which a head coil and the body model "Duke" from the Virtual Family dataset [11] is used. Hereafter, a pad design domain is defined

as a continuous layer covering the head with a thickness of 1 cm (Fig. 2b) which is subsequently divided into $D = 400$ rectangular subdomains as shown in Fig. 2c. Following the procedure described in [7], the matrices appearing in Eq. (5) are constructed, which in total contribute to 30 GB of disk storage.

As a next step, the snapshot matrix is filled column-wise by performing 2000 simulations in Remcom XFdtd with randomly chosen pad design parameters. The new reduced order basis is found by extracting the 500 most significant left singular vectors of the resulting snapshot matrix S. After performing the projections to find the new reduced order matrices of Eq. (8), the disk storage has been reduced to 1 GB only. The reduced order model allows us to evaluate B_1^+ fields in 0.35 seconds on a Windows 64-bit machine with an Intel Xeon CPU X5660 @ 2.80 GHz (dual core) with 48 GB internal memory and two NVIDIA Tesla K40c GPU's.

Having all the required matrices at our disposal, the dielectric pad for cerebellum imaging is optimized using Eq. (9) where a desired field intensity of 1.3 μT has been used. Within 10 iterations, which takes about 30 seconds, the optimal pad has been found with dimensions $32 \times 9.5 \times 1$ cm^3 and a relative permittivity of $\varepsilon_\mathrm{r} = 295$. The dielectric pad has been fabricated and tested in an MR experiment. The resulting T2-weighted map is shown in Fig. 1b. Comparing this scan with the scan obtained without a dielectric pad (Fig. 1a), it is evident that the contrast of the MR image has been improved.

4 CONCLUSIONS

In this paper, we have presented a pad optimization technique for improved high-field MR imaging. By introducing subdomains in a pad design domain, a set of suitably chosen pad design parameters, and by incorporating a model order reduction technique to remove possible field redundancies, we are able to design optimal dielectric pads in three dimensions for any imaging region of interest, typically within approximately one minute on a standard Windows 64-bit machine.

Acknowledgments

The research reported in this paper is financially supported by the Dutch Technology Foundation (STW, project number 13375).

References

[1] R. W. Brown, Y. N. Cheng, et al., *Magnetic resonance imaging: physical principles and sequence design*, 1st Edition, John Wiley & Sons, 1999, p. 6.

[2] P. F. Van de Moortele, C. Adriany, et al., "B1 destructive interferences and spatial phase patterns at 7 T with a head transceiver array coil," *Magn. Reson. Med.*, Vol. 54, No. 6, pp. 1503 – 1518, 2005.

[3] C. A. van den Berg, B. van den Bergen, et al. "Simultaneous B1+ homogenization and specific absorption rate hotspot suppression using a magnetic resonance phased array transmit coil," *Magn. Reson. Med.*, Vol. 57, No. 3, pp. 577 – 586, 2007.

[4] S. A. Winkler and B. K. Rutt, "Practical methods for improving B1+ homogeneity in 3 tesla breast imaging," *J. Magn. Reson. Imaging*, Vol. 41, No. 4, pp. 992 – 999, 2015.

[5] P. de Heer, W. M. Brink, B. J. Kooij, and A. G. Webb, "Increasing signal homogeneity and image quality in abdominal imaging at 3 T with very high permittivity materials," *Magn. Reson. Med.*, Vol. 68, No. 4, pp. 1317 – 1324, 2012.

[6] W. M. Brink, R. F. Remis, and A. G. Webb, "A theoretical approach based on electromagnetic scattering for analysing dielectric shimming in high-field MRI," *Magn. Reson. Med.*, Vol. 75, No. 5, pp. 2185 – 2194, 2016.

[7] J. H. F. van Gemert, W. M. Brink, A. G. Webb, and R. F. Remis, "An Efficient Methodology for the Analysis of Dielectric Shimming Materials in Magnetic Resonance Imaging," *IEEE Trans. Med. Imag.*, Vol. 36, No. 2, pp. 666 – 673, 2017.

[8] J. H. F. van Gemert, W. M. Brink, A. G. Webb, and R. F. Remis, "High-Permittivity Pad Design for Dielectric Shimming in Magnetic Resonance Imaging using Projection Based Model Reduction and a 3D Nonlinear Optimization Scheme," *IEEE Trans. Med. Imag.*, submitted, 2017.

[9] Quarteroni, Alfio, and Gianluigi Rozza. Reduced Order Methods for Modeling and Computational Reduction. Vol. 9. Springer, 2014.

[10] A. M. Batson, N. Petridou, et al., "Single session imaging of cerebellum at 7 Tesla: obtaining structure and function of multiple motor subsystems in individual subjects," *PLOS one*, Vol. 10, No. 8, 2015.

[11] A. Christ, "The Virtual Family development of surface-based anatomical models of two adults and two children for dosimetric simulations," *Phys. Med. Biol.*, Vol. 55, No. 2, pp. N23, 2010.